

# Giant exchange bias in a nanocomposite of BiFeO<sub>3</sub>-Bi<sub>2</sub>Fe<sub>4</sub>O<sub>9</sub>

Tuhin Maity and Saibal Roy\*

*Micropower-Nanomagnetics Group, Microsystems Center, Tyndall National Institute,  
University College Cork, Lee Maltings, Dyke Parade, Cork, Ireland*

Sudipta Goswami and Dipten Bhattacharya

*Nanostructured Materials Division, CSIR-Central Glass and Ceramic Research Institute, Kolkata 700032, India*

(Dated: February 28, 2012)

We report our observation of an enormous spontaneous exchange bias ( $\sim 40$ -60 mT) over a wide temperature range 5-300 K in a nanocomposite of BiFeO<sub>3</sub> ( $\sim 94\%$ )-Bi<sub>2</sub>Fe<sub>4</sub>O<sub>9</sub> ( $\sim 6\%$ ). It originates from the exchange coupling interaction between frozen superspin glass moments in Bi<sub>2</sub>Fe<sub>4</sub>O<sub>9</sub> (of average size  $\sim 19$  nm) and antiferromagnetism in BiFeO<sub>3</sub> (of average size  $\sim 112$  nm) across the interfaces and its magnitude decreases with either increase or decrease in the volume fraction of Bi<sub>2</sub>Fe<sub>4</sub>O<sub>9</sub>. The spin structure at the interface exhibits an interesting rearrangement dynamics under a magnetic training operation. This large exchange bias can be exploited for yielding a colossal "exchange bias mediated multiferroic coupling" between ferroelectricity in BiFeO<sub>3</sub> and magnetization in Bi<sub>2</sub>Fe<sub>4</sub>O<sub>9</sub> within such a nanocomposite.

PACS numbers: 75.70.Cn, 75.75.-c

Apart from the strong multiferroic coupling at room temperature,<sup>1</sup> BiFeO<sub>3</sub>, with a long wavelength ( $\sim 62$  nm) cycloidal magnetic structure and canted antiferromagnetism, exhibits an additional functionality of switching the magnetic anisotropy of a ferromagnetic layer<sup>2</sup> via exchange bias coupling in a BiFeO<sub>3</sub>-ferromagnetic layer composite. The switching can be triggered both by a magnetic as well as an electric field because of strong multiferroicity. The role of exchange bias coupling has been noted not just in a single crystal BiFeO<sub>3</sub>-ferromagnetic layer system but in other thin film based heterostructures as well, e.g., in BiFeO<sub>3</sub>/SrRuO<sub>3</sub>/SrTiO<sub>3</sub>/Si (001) [Ref. 3] or in BiFeO<sub>3</sub>/Co<sub>0.9</sub>Fe<sub>0.1</sub> [Ref. 4]. Whether the exchange bias is larger in thin film or in bulk BiFeO<sub>3</sub> based bilayer systems is debatable. While the exchange bias in thin films and nanoscale systems<sup>4</sup> originates from uncompensated cycloid of the magnetic structure, larger canting angle<sup>2</sup> offers significant exchange bias even in bulk BiFeO<sub>3</sub> based systems. We report in this paper that indeed in a naturally occurring (i.e., synthesized with minimum tailoring) nanocomposite of finer ( $\sim 19$  nm) Bi<sub>2</sub>Fe<sub>4</sub>O<sub>9</sub> and coarser ( $\sim 112$  nm) BiFeO<sub>3</sub>, both the spontaneous and conventional exchange bias (EB) are quite large ( $\sim 40$ -60 mT) across a wide temperature range 5-300 K and tunable via concentration ratio of the component phases. Interestingly, we discover that the exchange bias originates here not from conventional antiferromagnetic-ferromagnetic moment coupling interaction across the interfaces but from interaction between spin glass and antiferromagnetic structure. The magnitude of the exchange bias and the temperature zone across which it is observed vary depending on the concentration ratio of the phases in the nanocomposite.

The nanocomposite of BiFeO<sub>3</sub>-Bi<sub>2</sub>Fe<sub>4</sub>O<sub>9</sub> has been synthesized by sonochemical route where coprecipitation from aqueous solution of mixed metal nitrates takes place in presence of ultrasonic vibration. The precipitate thus

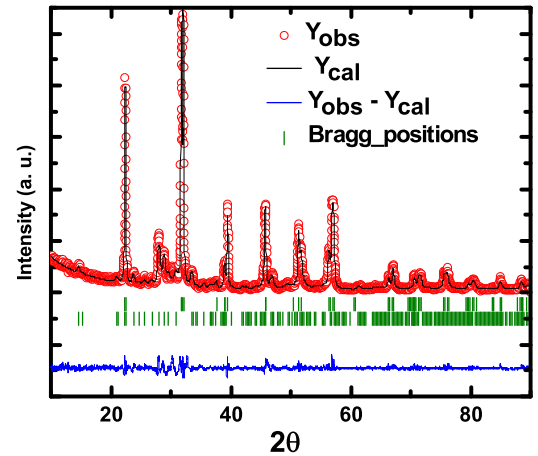


FIG. 1. (color online) The room temperature x-ray diffraction pattern of the nanocomposite. The pattern has been refined by FullProf.

formed is collected in a centrifuge running at 12000 rpm. The powder is finally washed, dried and calcined at 350-550°C for 4-5h in air. The parameters such as pH of the medium of coprecipitation, ultrasonic vibration energy, heat-treatment temperature, time etc can be controlled to yield nano-sized particles of either pure BiFeO<sub>3</sub> or a nanocomposite of BiFeO<sub>3</sub>-Bi<sub>2</sub>Fe<sub>4</sub>O<sub>9</sub> of varying concentration ratio of the component phases. The particle morphology and the crystallographic details have been studied by transmission electron microscopy (TEM), selected area electron diffraction (SAED), and high resolution transmission electron microscopy (HRTEM). The Rietveld refinement of the high resolution powder x-ray

TABLE I. Structural details of the phases in the nanocomposite from FullProf refinement of x-ray diffraction data.

Phase	Lattice Parameters (Å)	Ions	Wyckoff Positions	x	y	z	Bonds	Length (Å)	Bonds	Angle (°)	Crystallite Size	Volume Fraction
BiFeO <sub>3</sub> (R3c)	a = 5.579(5) c = 13.863(7)	Bi	6a	0.0	0.0	0.0	Bi-O	2.282(3)	Fe-O-Fe	152.19(7)	111.9	93.89
		Fe	6a	0.0	0.0	0.2251(5)	Bi-O	2.499(5)	O-Bi-O	72.36(4)		
		O	18b	0.4392(3)	0.01530(6)	-0.0482(4)	Fe-O	1.918(5)				
							Fe-O	2.165(3)				
Bi <sub>2</sub> Fe <sub>4</sub> O <sub>9</sub> (Pbam)	a = 7.976(6) b = 8.479(9) c = 6.008(3)	Bi	4g	0.1624(3)	0.1597(5)	0.0	Bi-O	2.461(3)	Fe-O-Fe	129.79(5)	19.3	6.11
		Fe1	4f	0.5	0.0	0.2669(3)	Bi-O	2.295(2)	O-Bi-O	65.72(3)		
		Fe2	8i	0.3682(5)	0.3356(7)	0.5	Bi-O	2.438(3)				
		O1	2b	0.0	0.0	0.5	Fe-O	2.092(4)				
		O2	8i	0.3722(7)	0.2147(6)	0.2425(6)	Fe-O	1.545(7)				
		O3	4f	0.1337(4)	0.4039(2)	0.5	Fe-O	2.016(4)				
		O4	4g	0.1534(6)	0.4303(6)	0.0						

diffraction pattern too offers information about the crystallographic details of the component phases in addition to the crystallite sizes and volume fraction of each phase. The magnetic measurements have been carried out in a SQUID magnetometer (MPMS, Quantum Design) across 5-300 K under a 5T magnetic field. While the spontaneous exchange bias (SEB) has been measured by studying the hysteresis loop at a given temperature without any magnetic annealing, conventional exchange bias (CEB) has been studied by conventional magnetic annealing treatment. Prior to any magnetic measurement, the sample has been demagnetized using an appropriate protocol.

We report here mainly the results obtained in a nanocomposite of ~6% Bi<sub>2</sub>Fe<sub>4</sub>O<sub>9</sub> and ~94% BiFeO<sub>3</sub> which exhibits maximum SEB and CEB. The increase or decrease in volume fraction of the Bi<sub>2</sub>Fe<sub>4</sub>O<sub>9</sub> phase from this optimum level gives rise to a sharp drop in the EB. In Fig. 1, the Rietveld refined x-ray diffraction patterns for the composite with optimum Bi<sub>2</sub>Fe<sub>4</sub>O<sub>9</sub> is shown. The crystallite sizes for the BiFeO<sub>3</sub> and Bi<sub>2</sub>Fe<sub>4</sub>O<sub>9</sub> phases turn out to be ~112 and ~19 nm, respectively, for this nanocomposite. The estimation from the x-ray diffraction data matches closely with what has been observed in TEM. Therefore, it appears that finer particles of Bi<sub>2</sub>Fe<sub>4</sub>O<sub>9</sub> are dispersed within the matrix of coarser BiFeO<sub>3</sub> particles. The structural details such as space group, lattice parameters, average <Bi-O>, <Fe-O> bond lengths, <O-Bi-O>, <Fe-O-Fe> bond angles, lattice distortion etc for the respective phases have also been determined and are given in Table-1. The spin structure of the individual phases (ferromagnetic, anti-ferromagnetic, spin glass etc) and that at the interface as well as the concentration of the interfaces are crucial in giving rise to the large spontaneous exchange bias observed. Detailed experiments have been carried out with TEM in order to investigate the concentration and nature of the interfaces between the particles of BiFeO<sub>3</sub> and

Bi<sub>2</sub>Fe<sub>4</sub>O<sub>9</sub>. In Fig.2a, we show a representative bright-field TEM image of the nanocomposite while in Figs. 2b and 2c, the representative dark-field (DF) - bright-field (BF) images of the individual particles and corresponding SAED and HRTEM images are shown. A large number of BF-DF TEM, SAED, and HRTEM images have been taken across different regions of the nanocomposite and analyzed in order to determine the concentration of the interfaces. It is interesting to observe that the finer Bi<sub>2</sub>Fe<sub>4</sub>O<sub>9</sub> particles are nearly evenly dispersed within the matrix of coarser BiFeO<sub>3</sub> particles thus maximizing the interface density. The SAED spots from the single crystalline BiFeO<sub>3</sub> and Bi<sub>2</sub>Fe<sub>4</sub>O<sub>9</sub> particles have been identified and indexed (Fig. 2d) accurately using the interplanar spacing (d) and angle ( $\phi$ ) data for the BiFeO<sub>3</sub> (space group R3c, hexagonal unit cell) and Bi<sub>2</sub>Fe<sub>4</sub>O<sub>9</sub> (space group Pbam, orthorhombic unit cell) phases. In the case of those spots which could be identified to be corresponding to a particular single crystal with a well-defined zone axis, the accuracy of indexing has been verified from the Weiss zone law<sup>5</sup> as well. Determination of the zone axes for the crystals of BiFeO<sub>3</sub> and Bi<sub>2</sub>Fe<sub>4</sub>O<sub>9</sub> yields the tilt across an interface as ~19° for a test case. However, since the particles are nano-sized and are oriented in different directions with respect to the beam direction, it is difficult to determine the zone axes for all such particles and find out the entire distribution pattern of orientation across the interfaces.

In Fig.3, the results from the magnetic measurements are shown. Once again, the results obtained for the composite with ~6 vol% of Bi<sub>2</sub>Fe<sub>4</sub>O<sub>9</sub> are, primarily, reported here. In Fig. 3a, we show the hysteresis loops measured at different temperatures across 5-300 K after reaching the desired temperature under zero-field cooling. The region near the origin is blown up to show the extent of EB clearly. In each case, the presence of a large shift in the loop - both along the field and magnetization axes - is conspicuous. Therefore, the EB here is spontaneous. The

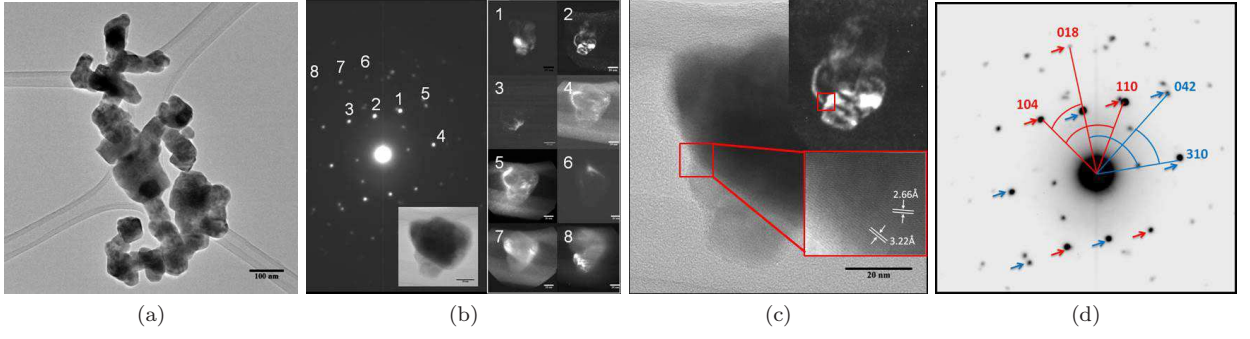


FIG. 2. (color online) (a) A representative bright-field TEM image of the nanocomposite; (b) the SAED patterns showing diffraction spots from both the phases; the dark-field images (marked by numbers) in the side panel shows the regions of the particles corresponding to the diffraction spots; inset shows the bright-field image of the region; the bright-field/dark-field images together with electron diffraction patterns from the regions show the dispersion of the phases and the interfaces in the nanocomposite; (c) a representative bright-field TEM image of an interface; top inset shows the dark-field image of the region while the bottom inset shows the HRTEM image of different orientation of the lattice fringes at the interface; (d) electron diffraction spots with their indexing corresponding to the pattern shown in (b); red and blue colors indicate the  $\text{BiFeO}_3$  and  $\text{Bi}_2\text{Fe}_4\text{O}_9$  phases, respectively.

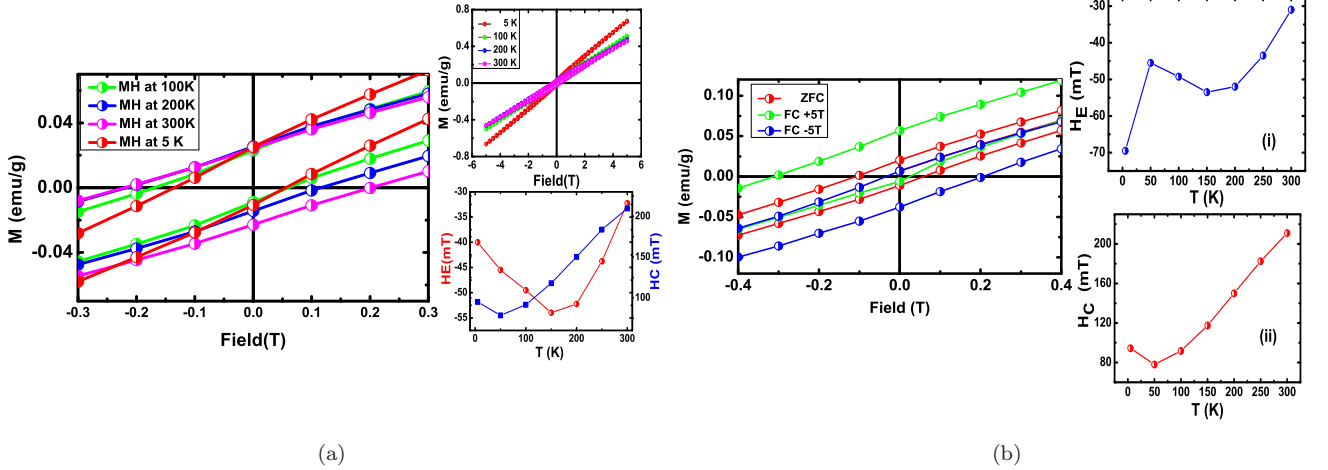


FIG. 3. (color online) (a) The spontaneous exchange bias observed at different temperatures across 5-300 K under zero-field cooling; the region near origin is blown up to show the extent of exchange bias clearly; side panel (i) shows the full hysteresis loops and side panel (ii) shows the variation of spontaneous  $H_E$  and  $H_C$  with temperature; (b) the conventional exchange bias observed under magnetic annealing at 5 K; it turns out to be negative in this case too; side panels (i) and (ii) show, respectively, the variation of conventional  $H_E$  and  $H_C$  with temperature.

EB  $H_E$  is given by  $(H_{c1} - H_{c2})/2$  while the coercivity  $H_C$  is given by  $(H_{c1} + H_{c2})/2$ ;  $H_{c1}$  and  $H_{c2}$  are the fields corresponding to the points in forward and reverse branches of the hysteresis loop at which the magnetization reaches zero. The magnitude of the SEB ( $\sim 40$ -60 mT) varies non-monotonically with the temperature; it increases with the increase in temperature till  $\sim 150$  K and then decreases with further increase in temperature. The extent of spontaneous EB observed here is larger than what has so far been reported for individual nanosized  $\text{BiFeO}_3$ <sup>6</sup> and  $\text{Bi}_2\text{Fe}_4\text{O}_9$ <sup>7</sup> particles with spatial inhomogeneity or core-shell structures. In fact, the magnitude across 5-300

K is even greater than what has so far been reported for any other thin film bilayer systems or nanocomposites.<sup>8</sup> In the top side panel of Fig. 3a, the entire hysteresis loop at a given temperature across  $\pm 5\text{T}$  is shown while in the bottom side panel the variation of the spontaneous exchange bias and coercivity with temperature is shown. The sign of the spontaneous EB depends on the sign of the starting field of the hysteresis loop tracing: if the starting field is  $+5\text{T}$  ( $-5\text{T}$ ), the EB turns out to be negative (positive). Therefore, the spontaneous EB appears to be negative here. In Fig. 3b, we show the CEB measured after a magnetic annealing treatment with either

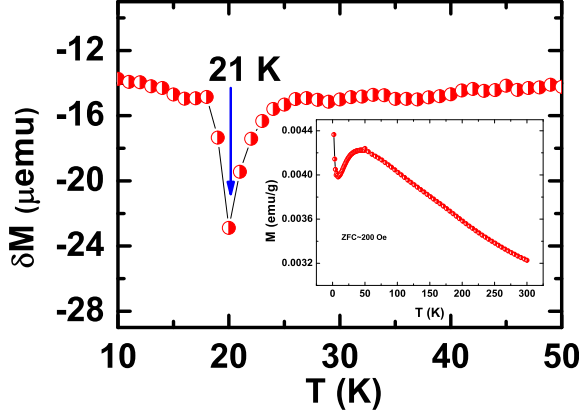


FIG. 4. (color online) The differential between two zero-field cooled magnetization versus temperature patterns recorded under two different protocols - a simple ZFC and a ZFC with stop and wait approach at 21 K; the dip in the differential is conspicuous proving the presence of superspin glass state in the composite; inset shows the reference line.

+5T or -5T. In the case of field-cooled or magnetic annealing mode measurements, a positive (negative) magnetic field of 5T has been applied at room temperature and then the temperature was ramped down to the given point at a cooling rate of 1 K/min. Like SEB, the CEB too turns out to be negative i.e., annealing under positive (negative) field yields hysteresis loop shift in negative (positive) direction along the field axis. As expected, the CEB depends on the magnetic history and is, therefore, tunable via different cooling field and ramping rate. In fact, the CEB increases linearly with the rise in annealing field right up to the field limit for our experiment 5T. In the side panels of Fig. 3b, we show the CEB and coercivity ( $H_C$ ) as a function of temperature measured under an annealing field of 1T. However, an interesting point here is that both the exchange bias  $H_E$  and cocercivity  $H_C$  for positive (negative) annealing field are asymmetric with  $|-H_E| > |+H_E|$ . *This is quite unusual for CEB.* The possible reasons could be a non-trivial interface spin structure and/or very small size of the antiferromagnetic domains.

In order to understand the origin of this phenomenon, we investigated the nature of the spin structure at the interface in detail from well designed protocol dependent magnetic moment versus temperature and magnetic training effect measurements. In this composite, the average size of the  $\text{BiFeO}_3$  particle is  $\sim 112$  nm. Therefore, the spin cycloid is complete and the bulk magnetization is nearly zero. The exchange energy is given by  $E_{ex} = \frac{1}{2} \vec{S}_F \vec{S}_{cant}$ . For a complete compensation in the antiferromagnetic spin structure, the exchange energy becomes zero. However, canted ( $\sim 1.6^\circ$  [Ref. 2]) as well as *locally* uncompensated spins may couple with the moments of finer ( $\sim 19$  nm)  $\text{Bi}_2\text{Fe}_4\text{O}_9$  through the interfaces. The

magnetic moment of the finer  $\text{Bi}_2\text{Fe}_4\text{O}_9$  particles embedded within antiferromagnetic  $\text{BiFeO}_3$  exhibits a rapid rise at low temperature (Fig. 4 inset). This is a signature of superparamagnetic moments.<sup>9</sup> The superparamagnetic domains could be frozen at a very low temperature and form superspin glass (SSG). Since it is difficult to confirm the presence of SSG in this case - as this structure, if present, is associated with the antiferromagnetism of  $\text{BiFeO}_3$  - we used a stop-and-wait protocol to measure the memory effect which is an unequivocal signature of presence of SSG.<sup>10</sup> The sample was first cooled down to 2 K from room temperature under zero field and an  $M(T)$  pattern (reference line) was measured under 200 Oe. After the sample temperature reaches 300 K, it was again brought back to 2 K under zero field. The  $M(T)$  measurement was then repeated but with a stop and wait protocol. As the temperature reaches at  $T_w \sim 21$  K, the measurement was stopped and waited at that temperature for  $\sim 10^4$  s. The difference between the two patterns  $\delta M(T)$  is shown in Fig. 4 main frame. The memory effect is shown as a dip at  $\sim 21$  K which confirms the presence of SSG in the nanocomposite.

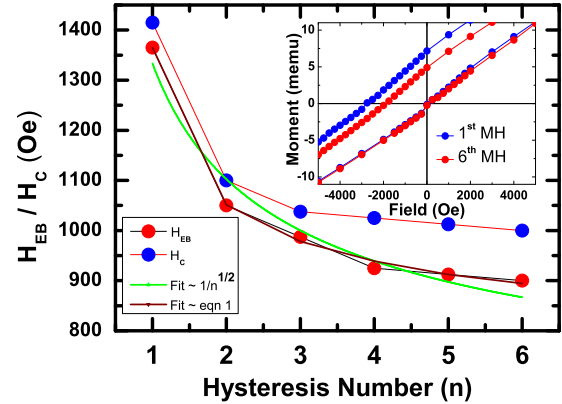


FIG. 5. (color online) The effect of training on the conventional exchange bias at 5 K. The exchange bias and coercivity decreases with the number of hysteresis cycles.

More details about the nature of spin structure at the interface could be obtained from a simple analysis of the repetitive training effect on CEB by measuring the hysteresis loops at 5 K repetitively using a protocol of field cooling under +5T. The dependence of  $H_E$  and  $H_C$  on the number of repeating cycles is shown in Fig. 5. Both the parameters are found to be decreasing monotonically with the increase in number of cycles indicating spin rearrangement at the interface. It appears that the empirical law<sup>11</sup> for purely antiferromagnetic spin rearrangement at the interface  $H_E^n = H_E^\infty + k \cdot n^{-\frac{1}{2}}$  with  $k = 788$  Oe and  $H_E^\infty = 544$  Oe cannot describe our data well (green line in Fig. 5). Instead, a model<sup>12</sup> which considers a mixed scenario of two different relaxation rates for frozen and rotatable uncompensated spin components at the interface  $H_E^n =$

$H_E^\infty + A_f \exp(-n/P_f) + A_i \exp(-n/P_i)$  (where  $f$  and  $i$  denote the frozen and interface spin components) fits the data perfectly well (brown line in Fig. 5) and yields the fitting parameters as  $H_E^\infty = 853$  Oe,  $A_f = 3244$  Oe,  $P_f = 0.39$ ,  $A_i = 370$  Oe, and  $P_i = 2.7$ . The ratio  $P_i/P_f \sim 8$  indicates that the interface spins rearrange nearly 8 times faster than the frozen spins. The exchange bias coupling thus develops here via interaction between antiferromagnetism in  $\text{BiFeO}_3$  and SSG in  $\text{Bi}_2\text{Fe}_4\text{O}_9$ . The interface region is populated by frozen and rotatable spin components which influence the SEB and CEB significantly. The exchange bias coupling in the case of ferromagnetic-spin glass heterostructure has earlier been shown by Ali *et al.*<sup>13</sup> Another interesting observation is the variation of both SEB and CEB with the concentration ratio of the component phases. As the volume fraction of the  $\text{Bi}_2\text{Fe}_4\text{O}_9$  phase decreases from  $\sim 6\%$  to  $\sim 3\%$ , the EB decreases drastically: the SEB drops down to  $\sim 0.1$  mT at 5 K and decreases monotonically with the rise in temperature while no CEB is observed. Likewise, increase in volume fraction ( $\sim 10\%$ ) of the  $\text{Bi}_2\text{Fe}_4\text{O}_9$  phase too, gives rise to a sharp drop in the SEB.

The giant SEB of  $\sim 60$  mT in a nanocomposite of  $\sim 6$  vol%  $\text{Bi}_2\text{Fe}_4\text{O}_9$  and  $\sim 94$  vol%  $\text{BiFeO}_3$  is a remarkable observation. Nearly 40 mT SEB has been observed even at room temperature in this composite which could be quite useful for storage devices. As determined from the TEM study, the concentration of the interfaces between the  $\text{BiFeO}_3$  and  $\text{Bi}_2\text{Fe}_4\text{O}_9$  particles is enormous with a nearly even distribution of finer particles within the matrix of coarser ones. In a test case, the tilt angle between the crystals of the phases turns out to be  $\sim 19^\circ$ . However, because of nano-size and different orientation of the crystals with respect to the beam direction, it is not possible to map the distribution of tilt angle across the entire matrix of the nanocomposite. Use of convergent beam electron diffraction with nano-diffraction images

could have been more suitable for the purpose. However, our TEM data clearly show that intimate mixing of the phases with large interface density does prevail in the nanocomposite which could be the origin of the observed giant EB. Interestingly, with further increase in the concentration of  $\text{Bi}_2\text{Fe}_4\text{O}_9$  phase, the interface density reduces because of large scale phase segregation and consequent drop in uniform dispersion of the phases. The large EB observed in the nanocomposite with optimum volume fraction of the phases adds a new functionality to the system. As demonstrated in Ref.2, exchange bias in  $\text{BiFeO}_3$ -permalloy layer system gives rise to "exchange bias mediated multiferroic coupling" between ferroelectricity of  $\text{BiFeO}_3$  and ferromagnetism of the permalloy layer. In the case of this nanocomposite, large EB is expected to increase the multiferroic coupling between  $\text{BiFeO}_3$  and  $\text{Bi}_2\text{Fe}_4\text{O}_9$  manyfold.

In summary, we report a giant spontaneous exchange bias of  $\sim 40$ - $60$  mT across 5-300 K as well as magnetic history dependent conventional exchange bias in a nanocomposite of  $\text{BiFeO}_3$  ( $\sim 94\%$ ) -  $\text{Bi}_2\text{Fe}_4\text{O}_9$  ( $\sim 6\%$ ). The exchange bias varies drastically with the variation in the concentration ratio of the component phases. Even though the spin cycloid in G-type antiferromagnetic  $\text{BiFeO}_3$  system is complete in particles of average size  $\sim 112$  nm, large canting as well as locally uncompensated spins offers local moment which couples with the superspin glass moments of nanosized  $\text{Bi}_2\text{Fe}_4\text{O}_9$ . This giant exchange bias can be utilized for improving the efficiency of electrical switching of magnetic anisotropy in a ferromagnetic system manyfold via "exchange coupling mediated multiferroicity".

This work has been supported by Indo-Ireland joint program (DST/INT/IRE/P-15/11) and FORME SFI SRC project (07/SRC/I1172) of Science Foundation of Ireland (SFI). One of the authors (S.G.) acknowledges support from CSIR Networked research program Nanostructured Advanced Materials (NWP051).

---

\* saibal.roy@tyndall.ie

- <sup>1</sup> D. Lebeugle, D. Colson, A. Forget, M. Viret, A.M. Bataille, and A. Gukasov, Phys. Rev. Lett. **100**, 227602 (2008).
- <sup>2</sup> D. Lebeugle, A. Mougin, M. Viret, D. Colson, and L. Ranno, Phys. Rev. Lett. **103**, 257601 (2009).
- <sup>3</sup> L.W. Martin, Y.-H. Chu, Q. Zhan, R. Ramesh, S.-J. Han, S.X. Wang, M. Warusawithana, and D.G. Schlom, Appl. Phys. Lett. **91**, 172513 (2007).
- <sup>4</sup> L.W. Martin, Y.-H. Chu, M.B. Holcomb, M. Hujiben, P. Yu, S.-J. Han, D. Lee, S.X. Wang, and R. Ramesh, Nano Lett. **8**, 2050 (2008).
- <sup>5</sup> See, for example, D.B. Williams and C.B. Carter,

*Transmission Electron Microscopy*, Part 2, Second Edition, (Springer, New York, 2009).

- <sup>6</sup> R. Mazumder, P.S. Devi, D. Bhattacharya, P. Choudhury, A. Sen, and M. Raja, Appl. Phys. Lett. **91**, 062510 (2007).
- <sup>7</sup> Z.M. Tian, S.L. Yuan, X.L. Wang, X.F. Zheng, S.Y. Yin, C.H. Wang, and L. Liu, J. Appl. Phys. **106**, 103912 (2009).
- <sup>8</sup> See, for example, J. Nogues and I.K. Schuller, J. Magn. Mater. **192**, 203 (1999).
- <sup>9</sup> D.Y. Cong *et al.*, Appl. Phys. Lett. **96**, 112504 (2010).
- <sup>10</sup> M. Sasaki *et al.*, Phys. Rev. B **71**, 104405 (2005).
- <sup>11</sup> D. Paccard *et al.*, Phys. Stat. Solid. **16**, 301 (1966).
- <sup>12</sup> S.K. Mishra *et al.*, Phys. Rev. Lett. **102**, 177208 (2009).
- <sup>13</sup> M. Ali *et al.*, Nature Mater. **6**, 70 (2007).